Mixed LoS/NLoS Near-Field Channel Estimation for Extremely Large-Scale MIMO Systems

Yu Lu and Linglong Dai

Department of Electronic Engineering, Tsinghua University,
Beijing National Research Center for Information Science and Technology (BNRist), Beijing 100084, China
Email: y-lu19@mails.tsinghua.edu.cn, daill@tsinghua.edu.cn

***Abstract*—Accurate channel estimation is essential to empower extremely large-scale MIMO (XL-MIMO) with ultra-high spectral efficiency in 6G networks. With the sharp increase in the antenna array aperture of the XL-MIMO system, the electromagnetic propagation field will change from far-field to near-field. Unfortunately, due to the near-field effect, the existing near-field XL-MIMO channel model mismatches the practical mixed line-of-sight (LoS) and non-line-of-sight (NLoS) channel feature. In this paper, a mixed LoS/NLoS near-field XL-MIMO channel model is proposed to accurately describe the LoS and NLoS path components simultaneously, where the LoS path component is modeled by the geometric free space propagation assumption while NLoS path components are modeled by the near-field array response vectors. Then, to define the range of near-field for XL-MIMO, the MIMO Rayleigh distance (MIMO-RD) is derived. Next, a two stage channel estimation algorithm is proposed, where the LoS path component and NLoS path components are estimated separately. Numerical simulation results demonstrate that, the proposed two stage scheme is able to outperform the existing methods.**

***Index Terms*—6G, extremely large-scale MIMO, channel estimation, near-field.**

I. Introduction

To achieve higher spectral efficiency, the extremely large-scale MIMO (XL-MIMO) is regarded as one of the most important technology for 6G [1], [2]. Since the antenna array aperture of XL-MIMO is very large, the receiver is more likely to lie in the near-field region of the transmitter, which is usually defined by the Rayleigh distance (RD) [3]. The RD is proportional to the square of the array aperture D and the inverse of wavelength $\frac{1}{\lambda}$. As the antenna number dramatically increases in XL-MIMO systems, the near-field range can be up to several hundreds of meters. In this case, the existing far-field channel estimation methods suffer from serious performance loss in the near-field XL-MIMO channel model. Thus, it is important to delicately model the XL-MIMO channel and design a near-field channel estimation scheme by analyzing the propagation property in the near-field XL-MIMO scenario [4].

The existing near-field channel estimation methods can be divided into two categories, i.e., MISO channel estimation [5], [6] and MIMO channel estimation. For the first category, the near-field MISO channel is modeled based on a near-field array response vector accurately, which relates not only to the angle but also to the distance due to the spherical wave assumption. Under this channel model, in [5], the whole two-dimensional plane is uniformly divided into multiple grids, and then the corresponding transform matrix can be constructed by multiple near-field array response vectors. With the constructed transform matrix, the near-field channel shows sparsity in the transform domain, which can be estimated by compressive sensing (CS)-based methods with low pilot overhead. The authors of [6] proved that the distance should be non-uniformly divided to reduce the correlation among the near-field array response vectors of the transform matrix. Based on the improved transform matrix, a new sparse representation in the polar-domain is proposed in [6] for XL-MIMO to increase the estimation accuracy.

The second category is based on the near-field XL-MIMO scenario, where the transmitter employs an extremely large-scale antenna array (ELAA) that serves receivers with multiple antennas or even an ELAA. For instance, an ELAA is installed on the top of a train [7], and the transmitter also deploys an ELAA. The authors of [8] draw on the experience of the far-field MIMO channel model and construct the near-field MIMO channel as the product of the transmitter and receiver near-field array response vectors. By utilizing the sparsity in the polar-domain, the CS-based method can be applied to the channel estimation problem under this channel model.

However, the existing near-field XL-MIMO channel model cannot accurately describe the near-field line-of-sight (LoS) path component. The reason is explained as below. In the far-field scenario, the transmitter with a small-aperture antenna array can be viewed as a point from the receiver and vice versa, where the transmitting and receiving processes are equivalent to two MISO propagation processes. Thus, the LoS path component can be represented by the product of transmitter and receiver array response vectors in the far-field scenario. However, in a near-field XL-MIMO system, due to the large aperture of ELAA, the receiver cannot be viewed as a point from the transmitter and vice versa. In this case, the existing near-field XL-MIMO channel model based on near-field array response vectors mismatches the practical XL-MIMO scenario in practice. Unfortunately, to the best of our knowledge, there is no study of this problem for XL-MIMO in the current literature.

To fulfill this gap, an accurate mixed LoS/NLoS near-field XL-MIMO channel model is first proposed, where the LoS path components and NLoS path components are modeled separately. Based on the proposed channel model, we derive the MIMO Rayleigh distance (MIMO-RD). Then, a two stage XL-

ICC 2023 - IEEE International Conference on Communications | 978-1-5386-7462-8/23/$31.00 ©2023 IEEE | DOI: 10.1109/ICC45041.2023.10278686

MIMO channel estimation scheme is proposed for the mixed LoS/NLoS near-field XL-MIMO channel model. Finally, we provide numerical simulation results to illustrate the effectiveness of our scheme.

II. System Model

In this section, the signal model of the near-field XL-MIMO system used in this paper will be introduced first. Then, we will review the existing near-field XL-MIMO channel model.

A. Signal Model

We consider that the transmitter and receiver are equipped with N_1-element and N_2-element antenna arrays, respectively. Since the antenna arrays are usually implemented in a digital-analog hybrid manner with a few RF (radio frequency) chains, we assume that RF chain numbers of the transmitter and receiver are $N_{\mathrm{t}}^{\mathrm{RF}}$ and $N_{\mathrm{r}}^{\mathrm{RF}}$. Let $\mathbf{H} \in \mathbb{C}^{N_2 \times N_1}$ denotes the channel from transmitter to receiver. The corresponding signal model can be presented as

$$\mathbf{y}_m = \mathbf{WHQ}\mathbf{s}_m + \mathbf{n}_m, \tag{1}$$

where $\mathbf{y}_m \in \mathbb{C}^{N_{\mathrm{r}}^{\mathrm{RF}} \times 1}$, $\mathbf{W} \in \mathbb{C}^{N_{\mathrm{r}}^{\mathrm{RF}} \times N_2}$, $\mathbf{Q} \in \mathbb{C}^{N_1 \times N_{\mathrm{t}}^{\mathrm{RF}}}$ and $\mathbf{s}_m \in \mathbb{C}^{N_{\mathrm{t}}^{\mathrm{RF}} \times 1}$ denote the received pilots signal, combining matrix, the hybrid precoding matrix, and transmitted signal in m-th times slots, and $\mathbf{n}_m \sim \mathcal{CN}\left(\mathbf{0}, \sigma^2 \mathbf{I}_{N_{\mathrm{r}}^{\mathrm{RF}}}\right)$ denotes the $N_{\mathrm{r}}^{\mathrm{RF}} \times 1$ received noise with σ^2 representing the noise power after combining in the m-th times slots.

Denote $\mathbf{p}_m = \mathbf{Q}\mathbf{s}_m \in \mathbb{C}^{N_1 \times 1}$, where the i-th element of the $\mathbf{p}_m$ is the signal transmitted by the i-th antenna at transmitter in m-th time slots. By collecting the received pilots in M time slots, we have

$$\mathbf{Y} = \mathbf{WHP} + \mathbf{N}, \tag{2}$$

where $\mathbf{Y} = [\mathbf{y}_1, \mathbf{y}_2, \ldots, \mathbf{y}_M]$, and $\mathbf{P} = [\mathbf{p}_1, \mathbf{p}_2, \ldots, \mathbf{p}_M]$ and $\mathbf{N} = [\mathbf{n}_1, \mathbf{n}_2, \ldots, \mathbf{n}_M]$. $\mathbf{Y} \in \mathbb{C}^{N_{\mathrm{r}}^{\mathrm{RF}} \times M}$, $\mathbf{W} \in \mathbb{C}^{N_{\mathrm{r}}^{\mathrm{RF}} \times N_2}$ and $\mathbf{P} \in \mathbb{C}^{N_1 \times M}$ denote the received pilots signal, combining matrix and the transmitted pilots signal in M times slots in a coherence interval, and $\mathbf{N} \sim \mathcal{CN}\left(\mathbf{0}, \sigma^2 \mathbf{I}_{N_{\mathrm{r}}^{\mathrm{RF}}} \otimes \mathbf{I}_M\right)$ denotes the $N_2 \times M$ received noise with σ^2 representing the noise power in M times slots. In channel estimation problem, we need to estimate $\mathbf{H}$ with given $\mathbf{P}$, $\mathbf{W}$ and $\mathbf{Y}$. To reduce the pilot overhead in a practical communication system, the channel estimation scheme with low overhead should be utilized $(M < N_1)$.

B. Existing Near-Field XL-MIMO Channel Model

For the existing near-field XL-MIMO channel model, similar to the far-field array response vectors based XL-MIMO channel model, the near-field array response vectors are utilized to replace the far-field array response vectors [8], which is presented as

$$\mathbf{H} = \sum_{l=1}^{L} g_l \mathbf{b}(\theta_r^l, d_r^l)\mathbf{b}^H(\theta_t^l, d_t^l), \tag{3}$$

where L denotes the number of path components, g_l represents the complex gain. $\mathbf{b}(\theta_t^l, d_t^l)$ and $\mathbf{b}(\theta_r^l, d_r^l)$ denote the near-field array response vectors at transmitter and receiver on the base of spherical wave assumption, which is denoted by

$$\begin{aligned}
\mathbf{b}(\theta_t^l, d_t^l) &= \frac{1}{\sqrt{N_1}}[e^{-j\frac{2\pi}{\lambda}(d_t^l(1)-d_t^l)}, \cdots, e^{-j\frac{2\pi}{\lambda}(d_t^l(N_1)-d_t^l)}]^H, \\
\mathbf{b}(\theta_r^l, d_r^l) &= \frac{1}{\sqrt{N_2}}[e^{-j\frac{2\pi}{\lambda}(d_r^l(1)-d_r^l)}, \cdots, e^{-j\frac{2\pi}{\lambda}(d_r^l(N_2)-d_r^l)}]^H,
\end{aligned} \tag{4}$$

where θ_t^l (θ_r^l) represent the angle for the l-th path at transmitter (receiver), and d_t^l (d_r^l) represent the distance of the l-th scatterer from the center of the antenna array of transmitter (receiver) for the l-th path, $d_t^l(n_1) = \sqrt{{d_t^l}^2 + \delta_{n_1}^2 d^2 - 2d_t^l \delta_{n_1} d \sin\theta_t^l}$ represents the distance of the l-th scatterer from the n_1-th element on transmitter antenna array, and $\delta_{n_1} = \frac{2n_1 - N_1 - 1}{2}$ with $n = 1, 2, \cdots, N_1$, and $d_r^l(n_2) = \sqrt{{d_r^l}^2 + \delta_{n_2}^2 d^2 - 2d_r^l \delta_{n_2} d \sin\theta_r^l}$ represents the distance of the l-th scatterer from the n_2-th transmitter antenna array, and $\delta_{n_2} = \frac{2n_2 - N_2 - 1}{2}$ with $n = 1, 2, \cdots, N_2$.

The polar-domain transform matrices can be presented as

$$\begin{aligned}
\mathbf{D}_t &= [\mathbf{b}(\theta_1, d_1^1), \cdots, \mathbf{b}(\theta_1, d_1^{S_1}), \cdots, \mathbf{b}(\theta_{N_1}, r_{N_1}^{S_{N_1}})], \\
\mathbf{D}_r &= [\mathbf{b}(\theta_1, r_1^1), \cdots, \mathbf{b}(\theta_1, d_1^{S_1}), \cdots, \mathbf{b}(\theta_{N_2}, r_{N_2}^{S_{N_2}})],
\end{aligned} \tag{5}$$

where each column of the matrix $\mathbf{D}_t$ $(\mathbf{D}_r)$ is a near-field array response vector sampled at angle $\theta_{n_1}(\theta_{n_2})$ and distance $d_{n_1}^{s_{n_1}}(d_{n_2}^{s_{n_2}})$, with $s_n = 1, 2, \cdots, S_{n_1}(S_{n_2})$. $S_{n_1}(S_{n_2})$ denotes the number of sampled distances at the sampled angle $\theta_{n_1}(\theta_{n_2})$. Therefore, we can calculate the total number of all sampled grids, i.e., the number of $\mathbf{D}_t$ $(\mathbf{D}_r)$ columns, which can be presented as $S_1 = \sum_{n_1=1}^{N} S_{n_1} (S_2 = \sum_{n_2=1}^{N} S_{n_2})$.

On the base of this polar-domain transform matrix $\mathbf{D}_t$ and $\mathbf{D}_r$, the channel $\mathbf{H}$ can be represented by

$$\mathbf{H} = \mathbf{D}_r \mathbf{H}^P \mathbf{D}_t^H, \tag{6}$$

where $\mathbf{H}^P$ is the $S_2 \times S_1$ polar-domain XL-MIMO channel, which also shows sparsity in the polar-domain.

This model is not suitable for the LoS path component in a near-field XL-MIMO scenario. Thus, in order to design the channel estimation algorithm for the XL-MIMO scenario, we should first provide an accurate description of the LoS path component, which will be described in Section III.

III. The Proposed Mixed LoS/NLoS Near-Field XL-MIMO Channel Model

In this section, we will first utilize the free space propagation assumption to accurately model the LoS path component for each transmitter-receiver antenna pair. Then, the mixed LoS/NLoS near-field XL-MIMO channel model is provided to capture the different features of LoS and NLoS path components, which are modeled separately.

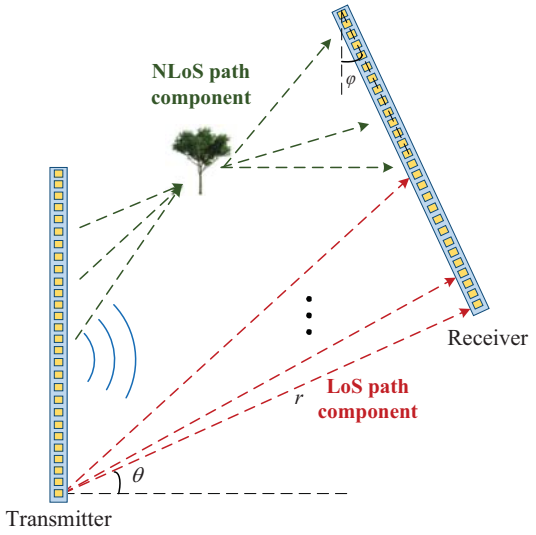

Fig. 1. The proposed near-field channel model for XL-MIMO.

A. LoS Path Component

For the near-field XL-MIMO LoS path component, each transmitter-receiver antenna pair will experience different propagation paths as shown in Fig. 1. Thus, in this case, the channel model built with the near-field array response vectors mismatches the practical feature of XL-MIMO near-field LoS path component. As a result, instead of utilizing near-field array response vectors like NLoS path components, we model the LoS path component under the geometric free space propagation assumption [9] for each transmitter-receiver antenna pair. Specifically, $\mathbf{H}(n_2, n_1)$ denotes the LoS path component of channel between the transmitter's n_1-th antenna and the receiver's n_2-th antenna, which can be represented as

$$\mathbf{H}(n_2, n_1) = \frac{1}{r_{n_2,n_1}} e^{-j\frac{2\pi}{\lambda} r_{n_2,n_1}}, \tag{7}$$

where r_{n_2,n_1} denotes the distance of the n_1-th antenna at receiver from the n_2-th antenna at transmitter. The r_{n_2,n_1} can be represented as

$$r_{n_2,n_1} = \sqrt{r^2 + d_1^2 + d_2^2 + 2rd_2\sin(\varphi+\theta) - 2rd_1\sin\theta - 2d_1d_2\cos\varphi} \tag{8}$$

where the r is the distance of the 1-st antenna at receiver from the 1-st antenna at transmitter, φ denotes relative angle between receiver and transmitter, and θ denotes the angle of departure (AoD) of the signal. Thus, by utilizing geometry relation in free space, the channel can be presented as

$$\mathbf{H}_{\text{LoS}} = \mathbf{H}_{\text{LoS}}(r, \theta, \varphi) = \left[\frac{1}{r_{n_2,n_1}} e^{-j2\pi r_{n_2,n_1}/\lambda}\right]_{N_2 \times N_1}, \tag{9}$$

Unlike the NLoS path components, the LoS path component cannot be decoupled by near-field array response vectors. Thus, the LoS path component cannot be presented by polar-domain channel with transform matrices.

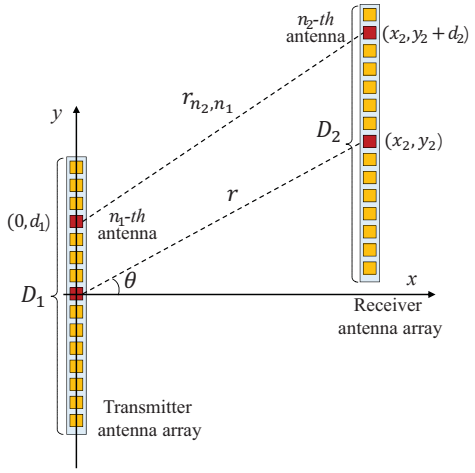

Fig. 2. The near-field MIMO scenario: antenna array elements (orange squares) in the *x*-*y* coordinate system

B. Proposed Mixed LoS/NLoS Near-Field XL-MIMO Channel

In order to capture both LoS and NLoS path components features, we propose a mixed LoS/NLoS near-field XL-MIMO channel model based on (6) and (9). The proposed XL-MIMO channel model can be presented:

$$\begin{aligned}\mathbf{H} &= \mathbf{H}_{\text{LoS}} + \mathbf{H}_{\text{NLoS}} \\ &= \mathbf{H}_{\text{LoS}}(r, \theta, \varphi) + \mathbf{D}_r \left(\sum_{l=1}^{L} g_l \mathbf{b}\left(\theta_r^l, d_r^l\right) \mathbf{b}^H\left(\theta_t^l, d_t^l\right)\right) \mathbf{D}_t^H.\end{aligned} \tag{10}$$

IV. The Definition of Rayleigh Distance for Near-Field XL-MIMO

In this section, we will define the MIMO Rayleigh distance (MIMO-RD) to determine the the boundary between the proposed mixed LoS/NLoS near-field XL-MIMO channel model and far-field MIMO channel model. As described in [3], the RD for a MISO scenario, i.e., MISO-RD, is defined as $Z = 2D^2/\lambda$, where D is the aperture of the antenna array and λ is the wavelength. MISO-RD is calculated by the condition that the largest phase discrepancy between the far-field planar wavefront and the near-field spherical wavefront in the free space is no more than $\pi/8$. However, the current MISO-RD is identified based on the scenario where only the transmitter employs the ELAA while the receiver is equipped with a single antenna. In this paper, by considering the XL-MIMO scenario, MIMO Rayleigh distance (MIMO-RD) is defined by the condition that the largest phase discrepancy between the far-field planar wavefronts and the near-field spherical wavefronts is no more than $\pi/8$.

As shown in Fig. 2, we consider the scenario where the transmitter and receiver are both equipped with antenna arrays of aperture D_1 and D_2, respectively. These two antenna arrays are set in parallel since the largest phase discrepancy occurs

when the wave impinges perpendicularly [10]. The center of transmitter antenna arrays is regarded as the $x-y$ coordinate origin. The coordinate of the n_1-th antenna of the transmitter antenna array, the center of receiver antenna array, the n_2-th antenna of the receiver antenna array are $(0, d_1)$, (x_2, y_2), and (x_2, y_2+d_2), respectively, where $-\frac{D_1}{2} \le d_1 \le \frac{D_1}{2}$ and $-\frac{D_2}{2} \le d_2 \le \frac{D_2}{2}$. The polar coordinate of the center of UE's antenna array can be written as $(r, \theta) = \left(\sqrt{x_2^2+y_2^2}, \arctan(\frac{y_2}{x_2})\right)$, where r, θ are the distance and angle between the center of transmitter's antenna array and the center of receiver's antenna array, respectively.

We only consider the phase change caused by LoS path component of the channel. As mentioned in (7), $\mathbf{H}(n_2, n_1) = \frac{1}{r_{n_2,n_1}} e^{-j2\pi r_{n_2,n_1}/\lambda}$ represents the LoS path component of channel between the transmitter's n_1-th antenna and the receiver's n_2-th antenna. r_{n_2,n_1} is the distance of the transmitter's n_1-th antenna from the receiver's n_2-th antenna. Here, the true phase is $\phi = \frac{2\pi}{\lambda} r_{n_2,n_1}$, where r_{n_2,n_1} is presented as

$$\begin{aligned} r_{n_2,n_1} &= \sqrt{x_2^2 + (y_2 + d_2 - d_1)^2} \\ &= r\sqrt{1 + \frac{(d_2-d_1)^2}{r^2} + \frac{2(d_2-d_1)\sin\theta}{r}}. \end{aligned} \tag{11}$$

where θ is the practical physical angle of departure. Specifically, by utilizing the second-order Taylor expansion $\sqrt{1+x} \approx 1 + \frac{1}{2}x - \frac{1}{8}x^2 + \mathcal{O}(x^2)$, we have

$$r_{n_2,n_1} \approx r + (d_2 - d_1)\sin\theta + \frac{(d_2-d_1)^2\cos^2\theta}{2r}. \tag{12}$$

Based on the far-field assumption, r_{n_2,n_1} can be approximated by its first-order Taylor expansion, where

$$r^{\text{far}}_{n_2,n_1} \approx r(1 + \frac{(d_2-d_1)\sin\theta}{r}) \quad = r + (d_2-d_1)\sin\theta \tag{13}$$

Thus, the far-field phase becomes $\phi^{\text{far}} = \frac{2\pi}{\lambda} r^{\text{far}}_{n_2,n_1}$. Accordingly, the phase discrepancy between the far-field planar and near-field spherical wavefronts can be presented as

$$\Delta = \left|\phi_{n_2,n_1} - \phi^{\text{far}}_{n_2,n_1}\right| = \frac{2\pi}{\lambda}\left|r_{n_2,n_1} - r^{\text{far}}_{n_2,n_1}\right| \tag{14}$$

Notice that $r^{\text{far}}_{n_2,n_1}$ in (13) is the first-order Taylor expansion of r_{n_2,n_1}, so $\left|r_{n_2,n_1} - r^{\text{far}}_{n_2,n_1}\right|$ in (14) is mainly determined by *the second-order Taylor expansion term of* r_{n_2,n_1}. Therefore, the phase discrepancy between planar wavefronts and spherical wavefronts is

$$\Delta \approx \frac{\pi(d_2-d_1)^2\cos^2\theta}{\lambda r}. \tag{15}$$

It can be observed that when $\theta = 0$, $d_1 = \frac{D_1}{2}(-\frac{D_1}{2})$ and $d_2 = -\frac{D_2}{2}(\frac{D_2}{2})$, phase discrepancy achieves maximum, where

$$\max \frac{\pi(d_2-d_1)^2\cos^2\theta}{\lambda r} = \frac{\pi(D_1+D_2)^2}{4r\lambda}. \tag{16}$$

Finally, since the largest phase discrepancy is larger than $\pi/8$ in the near-field region, we have

$$r \le \frac{2(D_1+D_2)^2}{\lambda}. \tag{17}$$

Thus, the MIMO-RD can be defined as $2(D_1+D_2)^2/\lambda$.

V. Proposed Two Stage Channel Estimation Algorithm

In this section, based on the proposed mixed LoS/NLoS near-field XL-MIMO channel model, we propose the two stage near-field XL-MIMO channel estimation algorithm.

A. Stage 1: LoS Path Component Estimation

Since the energy of the LoS path component is usually dominant, we will first conduct the LoS path component estimation. From (9), we can observe that the LoS path component of near-field MIMO channel is determined by three parameters, i.e., the distance of the 1-st antenna at receiver from the 1-st antenna at transmitter r, relative angle between receiver and transmitter φ, and the AoD θ. Therefore, the LoS path component estimation of (2) can be recognized as a parameter estimation problem, which can be presented as

$$\min_{r,\theta,\varphi} G(r,\theta,\varphi) \triangleq \|\mathbf{Y} - \mathbf{W}\mathbf{H}_{\text{LoS}}(r,\theta,\varphi)\mathbf{P}\|_F^2. \tag{18}$$

Algorithm 1 shows the procedure to solve the problem (18).

Algorithm 1 LoS path component estimation

Inputs: Received signal $\mathbf{Y}$, pilot $\mathbf{P}$, R_{max}, R_{min}, θ_{max}, θ_{min}, φ_{max}, φ_{min}, r_s, θ_s, φ_s, I.
Initialization: $\Delta r_1 = \frac{r_{max}-r_{min}}{r_s}$, $\Delta\theta_1 = \frac{\theta_{max}-\theta_{min}}{\theta_s}$, $\Delta\varphi_1 = \frac{\varphi_{max}-\varphi_{min}}{\varphi_s}$, calculate Ξ based on (19)
// Estimate coarse on-grid parameters
1. **for** $(r,\theta,\varphi) \in \Xi$ **do**
2. calculate $\mathbf{H}^*_{\text{LoS}}$ based on (9)
3. $r^{\text{int}}, \theta^{\text{int}}, \varphi^{\text{int}} = \underset{r,\theta,\varphi}{\text{argmin}} \|\mathbf{Y} - \mathbf{H}_{\text{LoS}}\mathbf{P}\|_2^2$
4. **end for**
// Refine off-grid parameters
5. **for** $i \in I$ **do**
6. update $\hat{r}^{(i+1)}$ based on (21)
7. update $\hat{\theta}^{(i+1)}$ based on (22)
8. update $\hat{\varphi}^{(i+1)}$ based on (23)
9. **end for**
10. $(r^{\text{opt}}, \theta^{\text{opt}}, \varphi^{\text{opt}}) = (\hat{r}^{(I)}, \hat{\theta}^{(I)}, \hat{\varphi}^{(I)})$
11. calculate $\hat{\mathbf{H}}_{\text{LoS}}$ based on (9) by $(r^{\text{opt}}, \theta^{\text{opt}}, \varphi^{\text{opt}})$
Output: Estimated LoS path component $\hat{\mathbf{H}}_{\text{LoS}}$.

First, in Steps1-4 we obtain on-grid coarse parameters by searching the collection Ξ, which can be presented as

$$\begin{aligned} \Xi = \{(r,\theta,\varphi) \,|\, & r = r_{\min}, r_{\min}+\Delta r, \cdots, r_{\max}; \\ & \theta = \theta_{\min}, \theta_{\min}+\Delta\theta, \cdots, \theta_{\max}; \\ & \varphi = \varphi_{\min}, \varphi_{\min}+\Delta\varphi, \cdots, \varphi_{\max}\}, \end{aligned} \tag{19}$$

where $r_{\min}$, $r_{\max}$, $\theta_{\min}$, $\theta_{\max}$, $\varphi_{\min}$, and $\varphi_{\max}$ represent the lower and upper boundaries of r, φ, and θ, respectively. Δr, $\Delta\theta$, and $\Delta\varphi$ are the step sizes of r, θ, and φ.

After searching the collection Ξ, we can get $r^{\text{int}}, \theta^{\text{int}}, \varphi^{\text{int}}$ as the initial on-grid estimated parameters. Then, to obtain the accurate estimated parameters, we refine three parameters $r^{\text{int}}, \theta^{\text{int}}, \varphi^{\text{int}}$ by iterative optimization method. Specifically, we define the objective function $G(r,\theta,\varphi)$ as

$$\min_{r,\theta,\varphi} G(r,\theta,\varphi) = \sum_{m=1}^{M} \mathbf{p}_m^H \mathbf{H}^H \mathbf{W}^H \mathbf{W} \mathbf{H} \mathbf{p}_m - \sum_{m=1}^{M} \left(\mathbf{p}_m^H \mathbf{H}^H \mathbf{W}^H \mathbf{y}_m + \left(\mathbf{p}_m^H \mathbf{H}^H \mathbf{W}^H \mathbf{y}_m \right)^H \right), \tag{20}$$

where the $\sum_{m=1}^{M} \mathbf{y}_m^H \mathbf{y}_m$ can be ignored since the $\mathbf{y}_m$ is fixed received signal.

The objective function $G(r,\theta,\varphi)$ can be optimized with an iterative gradient descent approach methods. In the i-th iteration, we need to calculate new estimated $\hat{r}^{(i+1)}$, $\hat{\theta}^{(i+1)}$, and $\hat{\varphi}^{(i+1)}$, which can be updated as

$$\hat{r}^{(i+1)} = \hat{r}^{(i)} - \eta_r \cdot \nabla_r G_{\text{opt}}^{(i)} \left(\hat{r}^{(i)}, \hat{\theta}^{(i)}, \hat{\varphi}^{(i)} \right). \tag{21}$$

$$\hat{\theta}^{(i+1)} = \hat{\theta}^{(i)} - \eta_\theta \cdot \nabla_\theta G_{\text{opt}}^{(i)} \left(\hat{r}^{(i)}, \hat{\theta}^{(i)}, \hat{\varphi}^{(i)} \right). \tag{22}$$

$$\hat{\varphi}^{(i+1)} = \hat{\varphi}^{(i)} - \eta_\varphi \cdot \nabla_\varphi G_{\text{opt}}^{(i)} \left(\hat{r}^{(i)}, \hat{\theta}^{(i)}, \hat{\varphi}^{(i)} \right). \tag{23}$$

η_r, η_θ, η_φ denote the lengths of step for the distance and angles to guarantee the $G_{\text{opt}}^{(i)} \left(\hat{r}^{(i+1)}, \hat{\theta}^{(i+1)}, \hat{\varphi}^{(i+1)} \right) \leq G_{\text{opt}}^{(i)} \left(\hat{r}^{(i)}, \hat{\theta}^{(i)}, \hat{\varphi}^{(i)} \right)$. The iteration process will suspend until reaching the largest iteration number.

Based on the $\left(\hat{r}^{(I)}, \hat{\theta}^{(I)}, \hat{\varphi}^{(I)} \right)$, we can obtain the estimated $\hat{\mathbf{H}}_{\text{LoS}}$ by (9). Then, we can eliminate the influence of $\hat{\mathbf{H}}_{\text{LoS}}$ on the received pilots $\mathbf{Y}$ and then estimate the $\hat{\mathbf{H}}_{\text{NLoS}}$, which is shown as follows.

B. Stage 2: NLoS Path Components Estimation

As we already acquire $\hat{\mathbf{H}}_{\text{LoS}}$, the received pilots without the effect of $\hat{\mathbf{H}}_{\text{LoS}}$ can be presented as

$$\mathbf{Y}_{\text{NLoS}} = \mathbf{Y} - \mathbf{W} \hat{\mathbf{H}}_{\text{LoS}} \mathbf{P}. \tag{24}$$

On the base of the polar-domain representation (6), the $\mathbf{Y}_{\text{NLoS}}$ can be presented as

$$\mathbf{Y}_{\text{NLoS}} = \mathbf{W} \mathbf{H}_{\text{NLoS}} \mathbf{P} + \mathbf{N} = \mathbf{W} \mathbf{D}_r \mathbf{H}_{\text{NLoS}}^P \mathbf{D}_t^H \mathbf{P} + \mathbf{N}. \tag{25}$$

As mentioned above, $\mathbf{H}_{\text{NLoS}}^P$ is sparse in polar-domain, thus the NLoS path components estimation is reformulated as a sparse recovery problem. In this sparse recovery problem, the NLoS path components sensing matrix at transmitter and receiver sides can be denoted as $\mathbf{A}_t = \mathbf{D}_t^H \mathbf{P}$ and $\mathbf{A}_r = \mathbf{W} \mathbf{D}_r$. The matrix OMP-based algorithm to solve this problem can be summarized in **Algorithm 2**.

Specifically, since there are L components in the polar-domain, we will conduct L iterations to find L supports in transmitter sensing matrix $\mathbf{A}_t$ and L supports in receiver sensing matrix $\mathbf{A}_r$. In l-th iteration, we will calculate the correlation between the transmitter and receiver sensing matrices $\mathbf{A}_t$, $\mathbf{A}_r$ and the residual matrix $\mathbf{R}$. In Step 4, we obtain the updated support Ω, Ω_1, Ω_2, where Ω_1, Ω_2 denote the support of transmitter and receiver sides. Then, in Step 6, the currently estimated near-field NLoS path component $\hat{\mathbf{h}}_A$ is calculated by the least square (LS) algorithm. In Step 7, the $\hat{\mathbf{h}}_A$ need to be reshaped into $\hat{\mathbf{H}}_A$ in the polar-domain of the size $S_2 \times S_1$. Finally, after L iterations are performed, we obtain the estimated NLoS path components $\hat{\mathbf{H}}_{\text{NLoS}}$.

Algorithm 2 NLoS path components estimation

Inputs: $\mathbf{Y}_{\text{NLoS}}$, $\mathbf{P}$, $\mathbf{W}$, $\mathbf{D}_r$, $\mathbf{D}_t$, L.
Initialization: $\Omega_1 = \emptyset$, $\Omega_2 = \emptyset$, $\Omega = \emptyset$, $\mathbf{A} = \mathbf{0}_{S_1 S_2 \times 1}$, $\mathbf{R} = \mathbf{Y}_{\text{NLoS}}$, $\mathbf{A}_t = \mathbf{D}_t^H \mathbf{P}$, $\mathbf{A}_r = \mathbf{W} \mathbf{D}_r$,
1. **for** $l = 1, 2, \cdots, L$ **do**
2. $n^* = \text{argmax} \| \text{vec}(\mathbf{A}_r{}^H \mathbf{R} \mathbf{A}_t{}^H) \|_2^2$
3. $n_1 = \text{floor}((n^* - 1)/N_2) + 1$, $n_2 = \mod(n^* - 1, N_2) + 1$
4. $\Omega = \Omega \bigcup n^*$, $\Omega_1 = \Omega \bigcup n_1$, $\Omega_2 = \Omega \bigcup n_2$
5. $\mathbf{A} = \left[\mathbf{A} \ \mathbf{A}_t(\Omega_1, :)^H \otimes \mathbf{A}_r(:, \Omega_2) \right]$
6. $\hat{\mathbf{h}}_A(\Omega) = (\mathbf{A}^H \mathbf{A})^{-1} \mathbf{A}^H \text{vec}(\mathbf{Y}_{\text{NLoS}})$
7. reshape $\hat{\mathbf{h}}_A$ into $\hat{\mathbf{H}}_A$ of size $S_2 \times S_1$
8. $\mathbf{R} = \mathbf{Y}_{\text{NLoS}} - \mathbf{A}_r \hat{\mathbf{H}}_A \mathbf{A}_t$
9. **end for**
10. $\hat{\mathbf{H}}_{\text{NLoS}} = \mathbf{D}_r \hat{\mathbf{H}}_A \mathbf{D}_t^H$
Output: Estimated NLoS path components $\hat{\mathbf{H}}_{\text{NLoS}}$.

After estimating the near-field LoS path component and the NLoS paths components, the $\hat{\mathbf{H}}$ can be written as

$$\hat{\mathbf{H}} = \hat{\mathbf{H}}_{\text{LoS}} + \hat{\mathbf{H}}_{\text{NLoS}}. \tag{26}$$

C. Computational Complexity Analysis

The computational complexity of the proposed two stage channel estimation algorithm can be analyzed as follows. In the stage of the LoS path component estimation, we can observe that the complexity comes from two parts, i.e., coarse on-grid estimation and refining processes. In Steps 1-4, for coarse on-grid estimation, we need to compute the $\mathbf{H}_{\text{LoS}}^*$ according to (9) in parameters collection, where the complexity of this part is $\mathcal{O}\left(S_{\text{LoS}} \left(N_{\text{r}}^{\text{RF}} N_1 N_2 + N_{\text{r}}^{\text{RF}} N_1 M \right) \right)$, where S_{LoS} is the size of the parameters collection. Then, for the refining process in Steps 5-9, the complexity is introduced by the gradient calculation. The complexity to calculate gradients $\mathcal{O}(MI(N_{\text{r}}^{\text{RF}} N_1 N_2 + N_{\text{r}}^{\text{RF}} N_1 + N_{\text{r}}^{\text{RF}} N_2 + N_2 N_1 + N_{\text{r}}^{\text{RF}}))$. Since the N_1, N_2 is usually much larger than N_{r}^{RF} and M, the complexity of the gradient calculation can be presented as $\mathcal{O}\left((S_{\text{LoS}} + MI) N_{\text{r}}^{\text{RF}} N_1 N_2 \right)$. For the NLoS path components estimation, the computational complexity can be obtained as $\mathcal{O}(N_1 N_2 (S_1 + S_2) L)$ by referring to the OMP algorithm [11].

VI. Simulation Result

In this section, we conduct the simulations to verify the performance of the proposed two stage channel estimation algorithm for the proposed mixed LoS/NLoS near-field XL-MIMO channel model. The system parameters are as follows: the number of antenna of transmitter and receiver are $N_1 = 256$ and $N_2 = 128$. The carrier frequency is $f = 50$ GHz, corresponding to $\lambda = 0.006\,\text{m}$. By utilizing (17), the MIMO-RD can be calculated as $\frac{2(D_1 + D_2)^2}{\lambda} = 442.7\,\text{m}$ in this scenario. The near-field channel in (3) contains $L = 3$ NLoS path components. Meanwhile, the sampled angles of arrival follow the uniform distribution $\mathcal{U}\left(-\frac{\pi}{3}, \frac{\pi}{3} \right)$.

Fig. 3 depicts the NMSE performance comparison with respect to the distance of the transmitter from the receiver. The

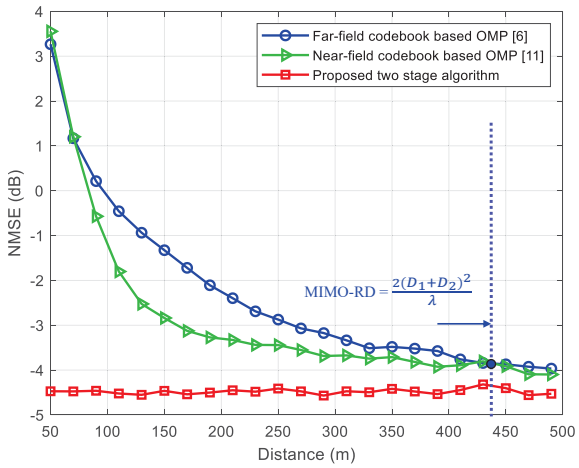

Fig. 3. NMSE performance comparison with respect to the distance of the transmitter from the receiver.

range of distance is from 50 m to 500 m. The SNR is 5dB and the size of pilot matrix is 256×128. The proposed two stage method can achieve better NMSE performance than the existing far-field codebook based OMP method [11] and the near-field codebook based OMP method [6]. Furthermore, we can observe that the MIMO-RD can capture the turning point of performance loss between the proposed two stage scheme and the far-field codebook based OMP scheme. Specifically, when the distance is larger than 442.7 m, the performance of the proposed two stage scheme and the far-field codebook based OMP channel estimation show the same performance. The reason is that when the distance is larger than MIMO-RD, the proposed channel model degenerates into the far-field channel model.

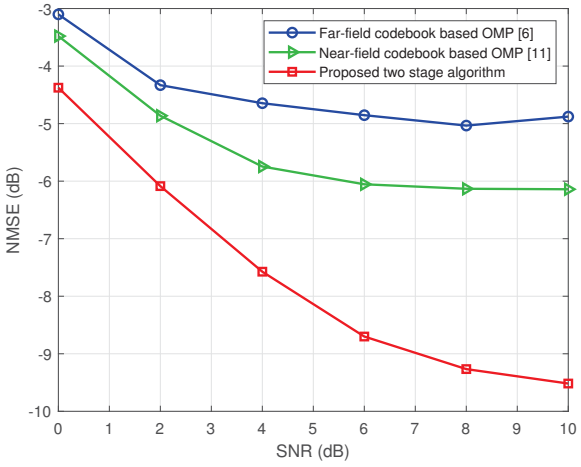

Fig. 4. NMSE performance comparison with respect to the SNR under $r = 60$ m.

Fig. 4 shows the NMSE performance comparison with respect to the SNR under different distances, the proposed scheme can achieve about 4 dB improvement compared with the near-field codebook based OMP scheme when SNR$= 0$ dB. The reason is that the existing near-field codebook based OMP schemes cannot deal with the LoS path component of the practical near-field XL-MIMO channel.

VII. Conclusions

In this paper, the channel estimation of the near-field XL-MIMO scenario was investigated. We proposed the mixed LoS/NLoS near-field XL-MIMO channel model, where the LoS and NLoS path components were characterized by geometric free space propagation assumption and the near-field response vectors, respectively. Then, we derived the range of the near-field region of XL-MIMO, i.e., MIMO-RD. Simulation results showed that, the proposed two stage channel estimation scheme achieved better NMSE performance than existing methods.

VIII. Acknowledgment

This work was supported in part by the National Key Research and Development Program of China (Grant No. 2020YB1807201), in part by the National Natural Science Foundation of China (Grant No. 62031019), and in part by the European Commission through the H2020-MSCA-ITN META WIRELESS Research Project under Grant 956256.

References

[1] E. D. Carvalho, A. Ali, A. Amiri, M. Angjelichinoski, and R. W. Heath, "Non-stationarities in extra-large-scale massive MIMO," *IEEE Wireless Commun.*, vol. 27, no. 4, pp. 74–80, Aug. 2020.

[2] V. Croisfelt, A. Amiri, T. Abrao, E. de Carvalho, and P. Popovski, "Accelerated randomized methods for receiver design in extra-large scale MIMO arrays," *IEEE Trans. Veh. Technol.*, vol. 70, no. 7, pp. 6788–6799, May 2021.

[3] K. T. Selvan and R. Janaswamy, "Fraunhofer and Fresnel distances: Unified derivation for aperture antennas," *IEEE Antennas Propag. Mag.*, vol. 59, no. 4, pp. 12–15, Aug. 2017.

[4] S. Sun, T. S. Rappaport, R. W. Heath, A. Nix, and S. Rangan, "MIMO for millimeter-wave wireless communications: beamforming, spatial multiplexing, or both?" *IEEE Commun. Mag.*, vol. 52, no. 12, pp. 110–121, Dec. 2014.

[5] Y. Han, S. Jin, C. Wen, and X. Ma, "Channel estimation for extremely large-scale massive MIMO systems," *IEEE Wireless Commun. Lett.*, vol. 9, no. 5, pp. 633–637, May 2020.

[6] M. Cui and L. Dai, "Channel estimation for extremely large-scale MIMO: Far-field or near-field," *IEEE Trans. Commun.*, vol. 70, no. 4, pp. 2663–2677, Apr. 2022.

[7] Z. Gong, C. Li, F. Jiang, and M. Z. Win, "Data-aided doppler compensation for high-speed railway communications over mmwave bands," *IEEE Trans. on Wireless Commun.*, vol. 20, no. 1, pp. 520–534, Jan. 2021.

[8] E. Zhou, H. Jiang, and H. Qi, "4-d parameter estimation in bistatic MIMO radar for near-field target localization," in *Proc. 2015 IEEE International Wireless Symposium (IWS'2015)*, 2015, pp. 1–4.

[9] J. Sherman, "Properties of focused apertures in the Fresnel region," *IEEE Trans. Antennas Propag.*, vol. 10, no. 4, pp. 399–408, Jul. 1962.

[10] E. Björnson, T. Demir, and L. Sanguinetti, "A primer on near-field beamforming for arrays and reconfigurable intelligent surfaces," in *Proc. 2021 55th Asilomar Conference on Signals, Systems, and Computers*, 2021, pp. 105–112.

[11] J. Lee, G. Gil, and Y. H. Lee, "Channel estimation via orthogonal matching pursuit for hybrid MIMO systems in millimeter wave communications," *IEEE Trans. Commun.*, vol. 64, no. 6, pp. 2370–2386, Jun. 2016.